TÜBİTAK

Turkish Journal of Physics

http://journals.tubitak.gov.tr/physics/

Research Article

Turk J Phys
(2013) 37: 99 – 106

doi:10.3906/fiz-1206-13

Investigation of dominant states in the collisions of Ar VII and Kr XXIV with H_2 and He targets

Abdel Aziz HABIB[1,*], **Alaa Abo ZALAM**[1], **Hassan RAMADAN**[2]
[1]Physics Department, Faculty of Science, Menoufia University, Menoufia, Egypt
[2]Basic Sciences Department, Faculty of Computer and Information Sciences,
Ain Shams University, Cairo, Egypt

Received: 19.06.2012 • **Accepted:** 29.08.2012 • **Published Online:** 20.03.2013 • **Printed:** 22.04.2013

Abstract: In thermal plasma, the ion–atom collisions proceed most probably through resonance processes. One of the important processes is the resonant transfer excitation followed by emission of X-rays (RTEX), which causes self-cooling for plasma. In addition, it is identical to the dielectronic recombination (DR) in electron–ion collisions. The present work deals with the calculation of DR cross-sections (σ^{DR}s) and DR rate coefficients (α^{DR}s) as well as RTEX cross-sections (σ^{RTEX} s) for Mg-like ions [Ar^{6+} and Kr^{24+}] with L-shell and K-shell excitation for $\Delta n = 0$ and $\Delta n \neq 0$. Comparison between the present results and other calculations for the rates are presented. RTEX cross-sections are calculated for the collision of Ar^{6+} and Kr^{24+} ions with He and H_2 targets. The calculations are carried out using the adapted angular momentum average scheme in the isolated resonance approximation.

Key words: Dielectronic recombination, resonant transfer excitation

1. Introduction

Dielectronic recombination (DR) is a process that plays an important role in plasma dynamics, and also is a subject of interest in studies of atomic structure. In astrophysical and fusion-related plasmas, DR is one of the dominant pathways for converting ions of charge q to a lower charge (q-1), and it is also responsible for DR satellite lines [1–3]. Accurate DR data are needed to interpret ionization structures of plasma [4], self-cooling of hot plasma, and plasma modeling. The DR process also governs the charge balance in atomic plasma [5–6].

Laboratory measurements can provide a small portion of the needed DR rate coefficients, but theoretical calculations are used to produce the bulk of the required DR data [7]. The rate coefficients are especially useful because they provide a good way to compare the importance of various multistep collisional or radiative processes. It is thus important to have accurate DR rate coefficients as well as many other atomic data for reliable plasma modeling, and also to make observations of such plasma. The DR rates are calculated for ions with initial excited states [8], or by using a semiempirical formula [9].

On the other hand, the process that takes place in ion–atom collisions is known as resonant transfer excitation (RTE) followed by X-ray (RTEX). Brandt [10] showed that RTEX in ion–atom collisions and DR in electron–ion collisions are identical processes when the restrictions of impulse approximation (IMA) are satisfied. He also formalized a mathematical relationship between RTEX and DR cross-sections using the Compton

*Correspondence: hramadan@eun.eg

profile of the momentum distribution of electrons in molecular H_2 or atomic He targets. The relationship between RTEX and DR cross-sections was applied in many theoretical works [11,12]. RTEX is successful in the explanation of the theoretical DR cross-sections, especially those with small values for $\Delta n \neq 0$ transitions. In addition, RTEX is still the main source for DR in highly charged positive ions.

This work aims to address DR cross-sections and DR rate coefficients as well as RTEX cross-sections where we focus on Ar^{6+} and Kr^{24+} (Mg-like ions) with L-shell (2p-) and M-shell (3s-) excitations. To avoid complexity, all needed Auger and radiative probabilities are calculated in the angular momentum average (AMA) scheme [13,14], in which all probabilities are averaged over both total orbital and total angular momenta for each intermediate state.

2. Theory

The DR process is completed in 2 successive steps that begin when an electron (of kinetic energy e_c and angular momentum ℓ) is captured by target ion ${X_i}^{(q)*+}$ (here, X_i stands for Ar^{6+} or Kr^{24+}) simultaneously with excitation of a bound state elicitation. The intermediate doubly excited resonance state ${X_d}^{(q-1)+}$ is formed, which may decay by emitting a photon to form a final bound state, thus completing the process of DR. The DR process can be expressed schematically as follows:

$$e_c + {X_i}^{(q)+} \rightarrow {X_d}^{(q-1)+**} \rightarrow {X_f}^{(q-1)+*} + \hbar\nu. \tag{1}$$

Similarly, the RTEX process is a 2-step process in which the ion captures an electron from an atom or molecule to form an intermediate doubly excited state (d-state). This process can be represented schematically as:

$${X_i}^{(q)+} + B \rightarrow {X_d}^{(q-1)+**} + B^+ \rightarrow {X_f}^{(q-1)+*} + B^+ + X - ray. \tag{2}$$

DR cross-sections (σ^{DR}) are calculated using the IMA within the framework of AMA to generate the RTEX cross-sections (σ^{RTEX}) for the collisions of Ar^{6+} and Kr^{24+} ions with H_2 and He targets. Bound states used in the calculations are obtained using the nonrelativistic single configuration Hartree–Fock approximation [12]. The continuum wave functions are obtained using the distorted wave approximation [12].

All doubly excited intermediate states formed with $\Delta n \neq 0$ and $\Delta n = 0$ excitations and contributing to the DR cross-section are presented in Table 1 for 2p-excitations and in Table 2 for 3s-excitations.

Table 1. The intermediate d-states that are formed with 2p-excitation for Mg-like ions, the final f-states reached by radiative decay, and Auger channels (j-states) reached by Auger decay from these intermediate states are presented. The ground i-state is $1s^2\,2s^2\,2p^6\,3s^2$.

j-states	d-states ($\Delta n \neq 0$)	f-states ($\Delta \ell = \pm 1$)
$1s^2 2s^2 2p^6 3sn'\ell'$	$1s^2 2s^2 2p^5 3s^2 n\ell n'\ell'$	$1s^2 2s^2 2p^6 3sn\ell n'\ell'$
$1s^2 2s^2 2p^6 3sn\ell$	(n = 3, 4)	$1s^2 2s^2 2p^6 3s^2 n'\ell'$
$1s^2 2s^2 2p^6 n\ell n'\ell'$	(ℓ = 0, 1, 2, 3)	$1s^2 2s^2 2p^6 3s^2 n\ell$
$1s^2 2s^2 2p^5 3s^2 n"\ell"$	(n' = 3, 4, 5, 6)	$1s^2 2s^2 2p^5 3s^2 n\ell^2$
	(ℓ' = 0, 1, 2, 3)	$1s^2 2s^2 2p^5 3s^2 n"\ell" n'\ell'$
		$1s^2 2s^2 2p^5 3s^2 n\ell n"'\ell"'$

Table 2. The intermediate d-states that are formed with 3s-excitation for Mg-like ions, the final f-states reached by radiative decay, and Auger channels (j-states) reached by Auger decay from these intermediate states are presented. The ground i-state is $1s^2\,2s^2\,2p^6\,3s^2$.

j-states	d-states ($\Delta n \neq 0$)	f-states ($\Delta \ell = \pm 1$)
$1s^2 2s^2 2p^6 3sn"\ell"$	$1s^2 2s^2 2p^6 3sn\ell n'\ell'$	$1s^2 2s^2 2p^6 3s^2 n'\ell'$
	(n = 3, 4)	$1s^2 2s^2 2p^6 3s^2 n\ell$
	($\ell = 0, 1, 2, 3$)	$1s^2 2s^2 2p^6 3sn"\ell" n'\ell'$
	(n' = 3, 4, 5, 6)	$1s^2 2s^2 2p^6 3s^2 n\ell^2$
	($\ell' = 0, 1, 2, 3$)	$1s^2 2s^2 2p^6 3s^2 n\ell n"'\ell"'$

The DR cross-section and rate coefficient are calculated by:

$$\bar{\sigma}^{DR} = [\frac{4\pi}{(p_0 a_0)^2}](\frac{Ry}{\triangle e_c})[\tau_0 V_a(i \rightarrow d)]\omega(d)(\pi(a_0)^2), \tag{3}$$

$$\bar{\alpha}^{DR} = [\frac{4\pi Ry}{kT}]^{3/2}(a_0)^3 V_a(i \rightarrow d)\omega(d)e^{-(\frac{e_c}{kT})}, \tag{4}$$

where p_0 is the momentum of the free electron, a_0 is the Bohr radius, τ_0 is the atomic unit of time that is given as $\tau_0 = 2.4189 \times 10^{-17}$ s, and $V_a(i \rightarrow\rightarrow d)$ and $\omega(d)$ are the radiationless capture probability and fluorescence yield respectively given by:

$$V_a(i \rightarrow d) = (\frac{g_d}{g_e g_i}) \sum_{i_c, \ell_c} A_a(d \rightarrow i_c \ell_c) \tag{5}$$

and

$$\omega(d) = \frac{\sum_f A_r(d \rightarrow f)}{\Gamma_a(d) + \Gamma_r(d).} \tag{6}$$

Here, the Auger and radiative transition probabilities A_a and A_r are the basic components of the cross-section given by:

$$A_a(d \rightarrow i) = (\frac{2\pi e^2}{\hbar a_0})|\langle i|\frac{1}{r_{12}}|d\rangle|^2 = \frac{2\pi}{\tau_0}|\langle i|\frac{1}{r_{12}}|d\rangle|^2, \tag{7}$$

where $\frac{1}{r_{12}}$ is the electron–electron coupling operator. On the other hand, the Auger width Γ_a is obtained by:

$$\Gamma_a(d) = [\Sigma_{i,\ell_c} A_a(d \rightarrow i, \ell_c) + \Sigma_{j,\ell'_c} A_a(d \rightarrow i, \ell'_c)]. \tag{8}$$

The single-electron radiative probability is given by:

$$A_r = \frac{2\pi}{\hbar}|\langle f|\hat{D}|d\rangle|^2 \rho_f, \tag{9}$$

where $\hat{D}$ is the photon–electron interaction operator and ρ_f is the density of final state. Moreover, the radiative width Γ_r is given by summing all the radiative probabilities for all final states of the corresponding intermediate state:

$$\Gamma_r(d) = \Sigma_f A_r(d \rightarrow f). \tag{10}$$

According to Eq. (2), atom B (H_2 or He) in ion–atom collision plays no role in the RTEX process. Since the Compton profile gives the probability of finding a particular target electron with a momentum p_z, it is utilized [10] with the IMA to relate the RTEX cross-section to the DR cross-section. The relationship between DR and RTEX cross-sections, following Brandt [10], is given by:

$$\bar{\sigma}^{RTEX} = \sqrt{\frac{M}{2E}} \triangle e_c J_B(p_z) \bar{\sigma}^{DR}, \tag{11}$$

where M is the mass of the projectile ion of energy E, $J_B(p_z)$ is the Compton profile, and p_z is the z-component of the momentum.

The calculations are concerned with L-shell (2p-) and M-shell (3s-) excitation for Ar^{6+} and Kr^{24+} ions. The d-state with L-shell excitation involves many Auger and radiative transitions in its stabilization. Thus, L-shell excitation needs longer calculations relative to M-shell excitation, which involves fewer Auger channels.

3. Results and discussions

3.1. DR cross-sections

The DR cross-sections for the collision of the projectile electron with Ar^{6+} and Kr^{24+} are calculated for the following 2 cases.

3.1.1. 2p-Excitation

The energy bin size is considered as Δe_c =1 Ry and 5 Ry for Ar^{6+} and Kr^{24+}, respectively. It is found that the dominant states in 2p-excitation are $1s^2 2s^2 2p^5 3s^2 3p5\ell$ with ℓ = 1, 2, and 3 for Ar^{6+} ion. They are $1s^2 2s^2 2p^5 3s^2 3dn\ell$ with n = 3, 4, and 5 and ℓ = 2 and 3 for Kr^{24+} ion.

3.1.2. 3s-Excitation

The DR cross-sections are calculated with Δe_c =1 Ry and 2 Ry for Ar^{6+} and Kr^{24+}, respectively. Too many states are affected in the cross-sections, such as the states $1s^2 2s^2 2p^6 3s4\ell n\ell'$ with ℓ = 0, 1 and 3 and ℓ' = 3, 4 for both ions.

3.2. DR rates

Eq. (4) was used to calculate the rate coefficients of Ar^{6+} and Kr^{24+} for 2p- and 3s-excitations under the validity of the isolated resonance approximation process.

3.2.1. 2p-Excitation

The variation of α^{DR} with kT (Ry) for Ar^{6+} is shown in Figure 1 as a comparison with α^{DR} for Kr^{24+} for 2p-excitation. It is found that the DR rates have a peak at kT = 20 Ry with $\alpha^{DR} = 2.51 \times 10^{-11}$ cm^3/s for Ar^{6+}. From Figure 1, it is clear that the peak value for Kr^{24+} is about 7.6 times larger than the peak value of Ar^{6+}, where α^{DR} peaks around kT = 90 Ry for Kr^{24+} such that the peak value is 1.91×10^{-10} cm^3/s.

3.2.2. 3s-Excitation

The variation of α^{DR} with kT (Ry) for Ar^{6+} is shown in Figure 2 as a comparison with the results of Loch et al. [15]. It is found that the DR rates peak around kT = 5 Ry with α^{DR} =8.33×10^{-11} cm^3/s. Figure 3

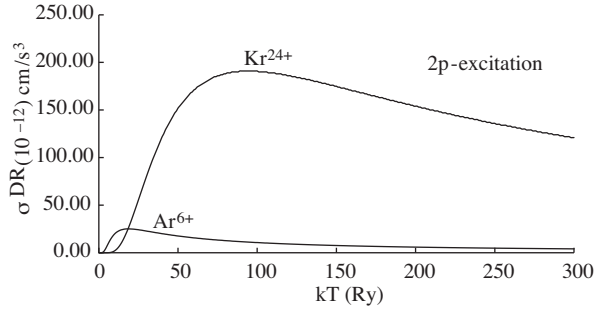

Figure 1. Comparison between the DR rate coefficients of Ar^{6+} and Kr^{24+} (cm^3/s) vs. kT (Ry) for 2p-excitation.

shows the variation of α^{DR} with kT (Ry) for Kr^{24+} as a comparison with the results of Altun [16], where the values peak around kT = 20 Ry with $\alpha^{DR} = 3.99 \times 10^{-10}$ cm^3/s. Our results for 3s-excitations for Ar^{6+}

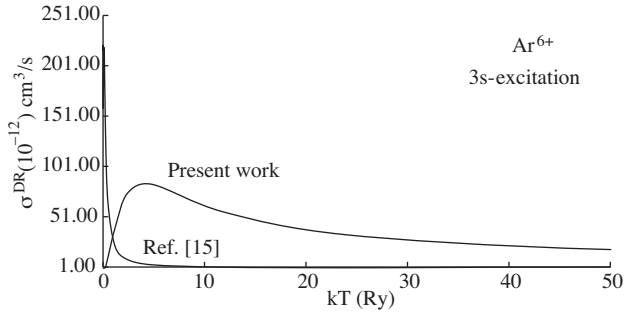

Figure 2. Comparison between the DR rate coefficients of Ar^{6+} for 3s-excitation for the present work and reference [15].

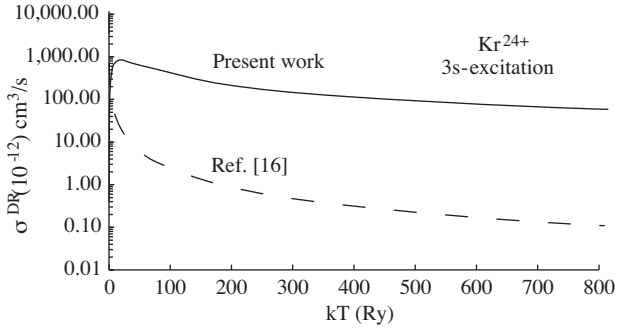

Figure 3. Comparison between the DR rate coefficients of Kr^{24+} for 3s-excitation for the present work and reference [16].

and Kr^{24+} ions are completely different from the results obtained in [15] and [16]. This is because there are no peaks shown in the results of [15] and [16], and so other calculations must have been performed with other schemes to clarify the rates.

3.3. RTEX cross-sections

3.3.1. Ar^{6+} ion

The RTEX cross-sections are calculated for Ar^{6+} with 2p- and 3s-excitations using the corresponding DR cross-sections.

σ^{RTEX}s are shown in Figure 4 for the collisions of Ar^{6+} with H_2 and He targets in case of 2p-excitation, while Figure 5 shows the results for 3s-excitations.

The RTEX cross-sections for Ar^{6+} with He is broader than that for Ar^{6+} with H_2. It is found that σ^{RTEX} for 3s-excitation is larger than that of 2p-excitation for the collision with H_2 and He targets. Moreover, σ^{RTEX} for 3s-excitation is about 7 times larger than that for 2p-excitation. Therefore, the RTEX process manifests itself as a more efficient mechanism for outer shells' excitations.

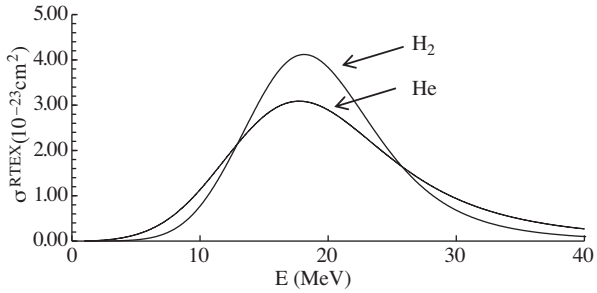

Figure 4. RTEX cross-sections in cm^2 for Ar^{6+} with H_2 and He for 2p-excitation.

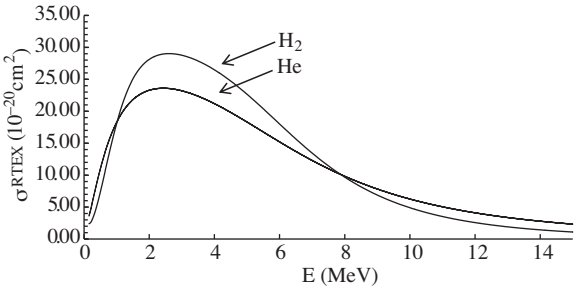

Figure 5. RTEX cross-sections in cm^2 for Ar^{6+} with H_2 and He for 3s-excitation.

3.3.2. Kr^{24+} ion

The RTEX cross-sections are calculated for Kr^{24+} with L-shell and M-shell excitations using the corresponding DR cross-sections.

The RTEX cross-sections for Kr^{24+} when it collides with both H_2 and He are given in Figure 6 for 2p-excitations. Moreover, Figure 6 shows that σ^{RTEX} has 2 peaks in the case of 2p-excitation. It is clear that the cross-section with He atom collision is broader than that with the H_2 molecule.

4. Conclusions

The work presented here deals with the theoretical aspects of the process known as DR's cross-sections and rate coefficients, as well as RTEX.

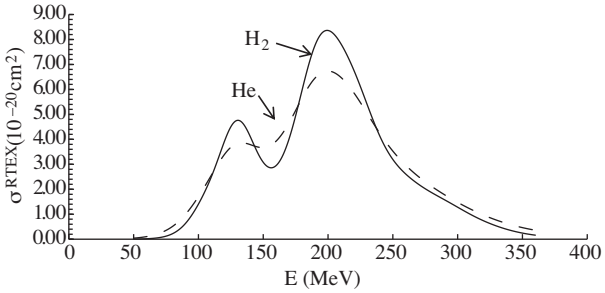

Figure 6. RTEX cross-sections in cm^2 for Kr^{24+} collisions with H_2 and He targets for 2p-excitation.

The results may be summarized as follows:

- There is a smooth variation for the DR rate coefficients with the temperature of the incident continuum electron for Ar^{6+} and Kr^{24+} ions. The antisymmetry around the peak values is verified for all curves of DR rates, which agrees with the Maxwellian distribution for the velocities of the continuum electrons.
- A severe difference was found between the present calculations and the calculations in references [15] and [16], which may be attributed to the following points: first, the explicit (step-by-step) calculation for a huge number of states as considered in Tables 1 and 2, and second, the arbitrarily estimated energy bin size Δe_c.
- The high Rydberg states contributions are considered and represented in all the calculations.
- The σ^{RTEX} for all ionic projectiles colliding with the He target is broader than that with H_2 target. However, the peak value of σ^{RTEX} decreases in the case of a He target.
- It is found that RTEX cross-sections for 3s-excitations are 7 times larger than that of 2p-excitations for the Ar^{6+} ion and 10 times larger in the case of Kr^{24+} for both targets H_2 and He.
- The range of projectile energies for RTEX cross-sections increases with the increasing of the atomic number Z of the ionic projectiles in the collisions with H_2 and He.
- The RTEX cross-sections for 3s-excitations exhibit a one-peak behavior for both Ar^{6+} and Kr^{24+}, as well as for 2p-excitations in the case of Ar^{6+}. However, a 2-peak behavior is found in Kr^{24+} with 2p-excitations, which reflects the nature of DR cross-sections for ions with high Z.

References

[1] P. Beiersdorfer, G. V. Brown, M. F. Gu, C. L. Harris, S. M. Kahn, S. H. Kim, P. A. Neill, D. W. Savin, A. J. Smith, S. B. Utter and K. L. Wong, *Proceeding of the International Seminar on Atomic Processes in Plasma, NIFS Proceedings Series No. NIFS-PROC-44*, ed. T. Kato and I. Murakami (National Institute for Fusion Studies, Nagoya, Japan, 2000), p. 25.

[2] K. J. H. Philips, J. Dubau, J. Sylwester and B. Sylwester, *Astrophys. J.*, **638**, (2006), 1154.

[3] D. W. Savin, *Rev. Mex. Astron. Astrofis.*, **9**, (2000), 115.

[4] D. W. Savin, B. Beck, P. Beiersdorfer, S. M. Kahn, G. V. Brown, M. F. Gu, D. A. Liedahl and J. H. Scofield, *Physica Scripta*, **T80**, (1999), 312.

[5] D. W. Savin, *J. Phys. Conf. Ser.*, **88**, (2007), 012071.

[6] N. R. Badnell, *J. Phys. Conf. Ser.*, **88**, (2007), 012070.

[7] http://www.adas.ac.uk/publications.php

[8] G. Omar and Y. Hahn, *Phys. Rev.*, **E63**, (2001), 46407.

[9] H. Ramadan, A. Khazbak and A. H. Moussa, *Z. Naturforsch.*, **58A**, (2003), 346.

[10] D. Brandt, *Phys. Rev.*, **A27**, (1983), 1314.

[11] H. Ramadan *Turk. J. Phys.*, **36**, (2012), 109.

[12] D. J. McLaughlin, I. Nasser and Y. Hahn, *Phys. Rev.*, **A31**, (1985), 1926.

[13] G. Omar and Y. Hahn, *Phys. Rev.*, **A44**, (1991), 483.

[14] K. LaGattuta, I. Nasser and Y. Hahn, *J. Phys. B: At. Mol. Phys.*, **20**, (1987), 1565.

[15] S. D. Loch, Sh. A. Abdel-Naby, C. P. Ballance and M. S. Pindzols, *Phys. Rev.*, **A76**, (2007), 022706.

[16] Z. Altun, A. Yumak, I. Yavuz, N. R. Badnell, S. D. Loch and M. S. Pindzola, *A&A*, **474**, (2007), 1051.